

SCIENTIFIC REPORTS



OPEN

Resonant Andreev Spectroscopy in normal-Metal/thin-Ferromagnet/Superconductor Device: Theory and Application

Received: 13 August 2015
Accepted: 02 November 2015
Published: 02 December 2015

Francesco Romeo¹, Filippo Giubileo², Roberta Citro^{1,2}, Antonio Di Bartolomeo¹, Carmine Attanasio^{1,2}, Carla Cirillo^{1,2}, Albino Polcari³ & Paola Romano^{3,2}

We develop a theoretical model to describe the transport properties of normal-metal/thin-ferromagnet/superconductor device. We perform experimental test of the model using a gold tip on PdNi/Nb bilayer. The resonant proximity effect causes conductance features very sensitive to the local ferromagnetic properties, enabling accurate measurement of polarization and thickness of the ferromagnet by point contact spectroscopy.

Spin polarization (P) represents an intrinsic parameter that characterizes a ferromagnet measuring the spin imbalance for the occupied electronic states. Experimentally, P can be determined by photoemission spectroscopy¹ (PS) as well as by spin-dependent spectroscopy on magnetic tunnel junctions² (MTJs), but both methods have important drawbacks: PS has limited energy resolution (few meV) and spatial sensitivity (few Angstrom of the surface) while MTJs need high quality fabrication process to get planar structures with uniform thin insulating barrier and a setup to apply high magnetic fields.

Less than twenty years ago, De Jong and Beenakker³ proposed the possibility to measure P by means of point contact Andreev reflection (PCAR) spectroscopy exploiting the Andreev reflection (AR) process at the metal(N)/superconductor(S) interface for which an incoming electron with energy less than the superconducting energy gap is retroreflected in the metal as a hole with opposite spin, while a Cooper pair enters the superconductor⁴. If the metal is a ferromagnet (F), the probability for AR is reduced and (transport) polarization can be obtained from the study of the differential conductance spectra, as experimentally reported in 1998 by Soulen *et al.*⁵ and by Upadhyay *et al.*⁶. Later, this technique has been used to characterize several ferromagnetic metals^{5–8} (Fe, Co, Ni), alloys^{5,9} (permalloy $\text{Ni}_x\text{Fe}_{1-x}$), manganites^{5,10,11} ($\text{La}_{1-x}\text{Sr}_x\text{MnO}_3$), ruthenates^{12,13} (SrRuO_3) and half metals^{5,14,15} (CrO_2).

From a theoretical point of view, a simple approach by Strijkers *et al.*⁷ gives a generalization of the Blonder-Tinkham-Klapwijk (BTK) theory¹⁶ to spin polarized materials by considering the current flowing in a F/S contact as $I = (1 - P) \cdot I_u + P \cdot I_p$ with I_p and I_u the fully polarized and fully not-polarized current, respectively. Their model considers a weak (proximized) superconducting layer at the interface and succeeded, in some cases, to fit conductance dips often experimentally observed at energies close to the gap energy. Alternatively, F. Pérez-Willard *et al.*¹⁷ have considered two spin-dependent transmission coefficients for the majority and minority carriers in the ferromagnet. Both models have been widely applied to extract spin polarization in several PCAR experiments involving ferromagnetic materials. This powerful method probes the bulk polarization of the ferromagnet (used as one of the electrodes) in the F/S contact. In this case, the boundary conditions are determined by the bulk density of states (DOS) in F, and consequently the Andreev reflection probability is reduced by the lack of DOS available for the electron-hole scattering.

¹Dipartimento di Fisica "E. R. Caianiello", Università di Salerno, Fisciano, Italy. ²CNR-SPIN Salerno, via Giovanni Paolo II 132, Fisciano, Italy. ³Dipartimento di Scienze e Tecnologie, Università del Sannio, Benevento, Italy. Correspondence and requests for materials should be addressed to F.R. (email: fromeo@sa.infn.it)

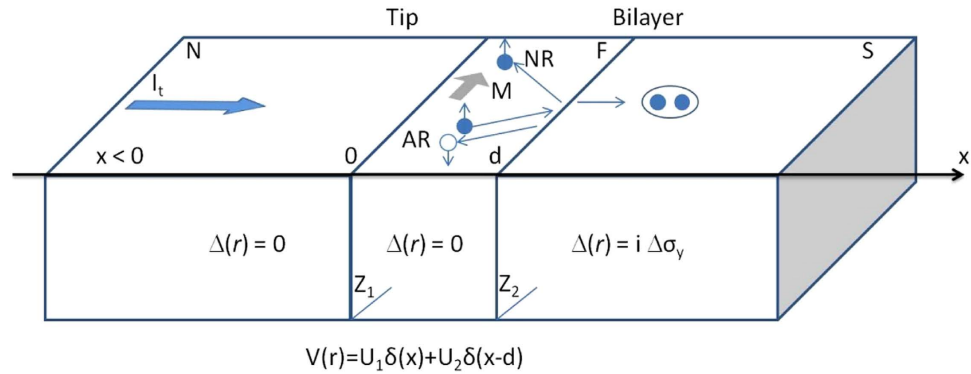


Figure 1. Schematic representation of a Resonant Andreev Spectroscopy setup. Transport current I_t flows from metallic tip through N/F (parameterized by Z_1) and then F/S (Z_2) interfaces, barrier strengths depending on the scattering potential $V(r)$. Ferromagnetic region ($0 < x < d$) has magnetization M perpendicular to transport direction. Superconducting pairing potential $\Delta(r)$, existing in S, causes Andreev reflection (AR), while the normal reflection (NR) at F/S and N/F interface is caused by $V(r)$.

The scenario described above is modified when PCAR spectroscopy is used to characterize F/S bilayers where a thin F-layer covers the S-electrode, a configuration of technological interest in the field of magnetic nano-devices. The analysis of such system requires further theoretical investigations, specially in the presence of very thin ferromagnetic layer. Indeed, the use of metallic (non-magnetic) tip as electrode realizes a N-F/S device in which the N-electrode fixes the boundary conditions. In this case, the Andreev probability is not limited by the lack of DOS, as for a bulk ferromagnetic electrode configuration, while it is strongly affected by interference phenomena caused by resonant proximity effect. The resonant proximity originates from the influence of Andreev bound states confined to the F-layer and can be extremely sensitive to the ferromagnetic properties (thickness and polarization). For these reasons, resonance effects can be exploited to implement a Resonant Andreev Spectroscopy technique useful for the characterization of magnetic systems of reduced dimensions.

In this work we develop a theoretical model within the Bogoliubov-de Gennes (BdG) formalism¹⁸ taking into account the presence of the tip/sample (N/F) and F/S (in the bilayer) interface, which correctly reproduces the double barrier geometry of a Resonant Andreev Spectroscopy setup. The theory demonstrates that N-F/S configuration allows precise estimation of spin polarization as well as of the ferromagnet local thickness. A first evidence of the applicability of the model is provided by analyzing results obtained in PCAR experiment using a gold tip on the ferromagnetic side of a PdNi/Nb bilayer.

Results

Theoretical model. Up to now, double barrier problem, relevant in describing a Resonant Andreev Spectroscopy setup, has been studied for diffusive N/X/S systems (with X indicating a normal metal or a ferromagnet) by using Usadel equations^{19,20}. The semiclassical nature of this approach²¹ requires the existence of a semiclassical solution in the interlayer which is only allowed for a minimum interlayer thickness (i.e. the distance between the two barriers) much larger than the Fermi-wavelength. For smaller thickness, the double barrier transmission coefficients are strongly affected by quantum-mechanical coherence. Thus, for the N-F/S system with reduced thickness of the F-interlayer ($\sim \xi_F$, where ξ_F is the characteristic length of the superconducting correlation decay in the F-layer), we adopt a Bogoliubov-de Gennes formalism in which the wave function $\Psi(r)$, describing an excitation of energy E in the tip, in the ferromagnetic layer or in the superconductor, is derived by solving the eigenvalues problem given by ($x \neq 0, d$)

$$\begin{bmatrix} H(r) & \Delta(r) \\ \Delta^\dagger(r) & -H^*(r) \end{bmatrix} \Psi(r) = E \Psi(r). \quad (1)$$

In Fig. 1 we give a schematic of the model. The picture evidences the three-dimensional character of the bulk normal electrode (tip) which provides the correct boundary condition for the scattering problem of electronic processes generated asymptotically far from the interface. This is the standard procedure applied in the scattering theory and used in the BTK approach¹⁶: the scattering coefficients are calculated by considering the normal tip as a layer of infinite transverse dimension^{22–24}, as detailed hereafter.

The tip region ($x < 0$), does not present superconducting correlations ($\Delta(r) = 0$), while $H(r) = -\frac{\hbar^2 \nabla^2}{2m} - E_F \equiv H_0(r)$ is the tip quasi-particle Hamiltonian. The thin ferromagnetic layer ($0 < x < d$) is modeled by adding to $H_0(r)$ a Zeeman energy term, $-g\mu_B M \hat{\sigma}_z \equiv -E_F \hbar \hat{\sigma}_z$, describing a

magnetization M belonging to the $y-z$ easy plane orthogonal to the transport direction (x -direction). The superconducting region ($x > d$) is described by a homogeneous pairing potential $\Delta(r) = i\Delta\hat{\sigma}_y$. The Fermi velocities mismatch among the different regions and the non-ideality of the interfaces are modeled by using a scattering potential $V(r) = U_1\delta(x) + U_2\delta(x-d)$, $\delta(x)$ being the Dirac delta function. The translational invariance implies the conservation of the linear momentum $\hbar\mathbf{k}_{\parallel} \equiv \hbar(0, k_y, k_z)$ parallel to the interface. Thus, the wave function in each region can be written in the form $\Psi(r) = e^{i(k_y y + k_z z)} \psi(x|E, \mathbf{k}_{\parallel})$ leading to an effective one-dimensional problem for $\psi(x|E, \mathbf{k}_{\parallel})$, being the energy E and \mathbf{k}_{\parallel} conserved quantum numbers during a scattering event. Once the wave functions $\psi_t(x|E, \mathbf{k}_{\parallel})$, $\psi_f(x|E, \mathbf{k}_{\parallel})$ and $\psi_s(x|E, \mathbf{k}_{\parallel})$ describing, respectively, the tip, the magnetic layer and the superconductor have been expressed in terms of eigenfunctions associated to the eigenvalues problem given in equation (1), the scattering coefficients are determined by imposing the boundary conditions:

$$\psi_t(x=0|E, \mathbf{k}_{\parallel}) = \psi_f(x=0|E, \mathbf{k}_{\parallel}) \quad (2)$$

$$\psi_s(x=d|E, \mathbf{k}_{\parallel}) = \psi_f(x=d|E, \mathbf{k}_{\parallel}) \quad (3)$$

$$\partial_x \psi_f(x|E, \mathbf{k}_{\parallel})|_{x=0} - \partial_x \psi_t(x|E, \mathbf{k}_{\parallel})|_{x=0} = k_F Z_1 \psi_t(x=0|E, \mathbf{k}_{\parallel}) \quad (4)$$

$$\partial_x \psi_s(x|E, \mathbf{k}_{\parallel})|_{x=d} - \partial_x \psi_f(x|E, \mathbf{k}_{\parallel})|_{x=d} = k_F Z_2 \psi_f(x=d|E, \mathbf{k}_{\parallel}), \quad (5)$$

where k_F indicates the Fermi wave vector, while $Z_{1/2}/2 = mU_{1/2}/(\hbar^2 k_F)$ represents the BTK parameter describing the interface properties. The current I_t flowing through the device is expressed via the AR coefficients $a_{\sigma'\sigma}(E, \mathbf{k}_{\parallel})$ and the normal reflection coefficients $b_{\sigma'\sigma}(E, \mathbf{k}_{\parallel})$ defining the tip wave function $\psi_t = \psi_{e\sigma}^{in} + \sum_{\sigma'} b_{\sigma'\sigma} \psi_{e\sigma'}^{out} + \sum_{\sigma'} a_{\sigma'\sigma} \psi_{h\sigma'}^{out}$. Here ψ_t is decomposed into incoming (in) or outgoing (out) electron-like ($\psi_{e\sigma}^{in/out}$) and hole-like ($\psi_{h\sigma}^{in/out}$) modes having spin projection $\sigma\hbar/2$, with $\sigma = \pm 1$.

Fixing the wave vector modulus $k(E) = \sqrt{2mE}/\hbar \approx k_F$, and changing the integration variables, i.e. $\int d^2\mathbf{k}_{\parallel} \rightarrow \int k^2(E) (\sin\phi)^2 \cos\theta d\theta d\phi$, the differential conductance can be derived as $G(V) = \frac{dI_t}{dV}$ from

$$I_t(V) \propto \frac{k_F^2 \mathcal{A}}{(2\pi)^2} \int dE d\Omega \mathcal{D}(E, \theta, \phi) \left[2 + \sum_{\sigma\sigma'} |a_{\sigma'\sigma}(E, \theta, \phi)|^2 - \sum_{\sigma\sigma'} |b_{\sigma'\sigma}(E, \theta, \phi)|^2 \right] \times (f(E - eV) - f(E)), \quad (6)$$

where $f(E)$ is the Fermi-Dirac distribution, \mathcal{A} represents the tip cross section, $d\Omega \equiv (\sin\phi)^2 \cos\theta d\theta d\phi$, while the angular integration is performed over the incidence angles $\theta \in [-\pi/2, \pi/2]$ and $\phi \in [0, \pi]$. The factor $\frac{k_F^2 \mathcal{A}}{(2\pi)^2}$ counts the number of transverse modes which participate in the charge transport in the bulk. The finite dimension of the contact (N/F), naturally not included in the asymptotic boundary conditions of the scattering problem, is usually taken into account by introducing the tip shape factor $\mathcal{D}(E, \theta, \phi)$ in the current calculation as an exponential²³ or a Lorentzian²⁴ weight. This introduces one more model parameter related to the acceptance tunneling cone. When the spectroscopic features are not significantly affected by the introduction of such weight factor, it is usually neglected in order to simplify the model considering only parameters directly connected to physical measurable quantities. In the BTK formalism, the tip geometry information can be alternatively introduced by limiting the angular integration range (as we did in the calculations) to a maximum incidence angle (rectangular weight factor) defining the tunneling cone. Mathematically, the equivalence of the two procedures is expected for low transparency barriers (high Z values), because in such a case the high angle transmission processes are strongly suppressed²⁴.

The normalized differential conductance spectra $G(V)/G_{NN}$ (with $G_{NN} = G(V)|_{eV \gg \Delta}$) are the physical observables to be compared with the experimental data.

The theoretical model, despite its ballistic nature, is expected to correctly describe physical systems with subdominant diffusive contributions. Indeed, the particle trajectories which contribute to the tunneling current can be classified in two groups: (i) particle trajectories with a scattering angle close to the interface normal direction; (ii) particle trajectories with high incidence angle exploring the transverse dimension of the F layer. The (i)-type trajectories provide the coherent contribution to the tunneling current and retain the quantum mechanical information described by the Bogoliubov-de Gennes formalism (ballistic); (ii)-type trajectories are representative of the diffusive motion along the transverse direction and provide an additive incoherent resistance. This featureless (energy insensitive) spectroscopic background contribution is usually accounted adding a classical resistance to the model, as we did in the calculations. Consequently, the use of a ballistic formalism, corrected by a classical (incoherent) contribution, is suitable for the correct modelling of the physical system. We stress that the BTK theory as well as the several generalized versions of it typically refer to the ballistic description of the phenomenon,

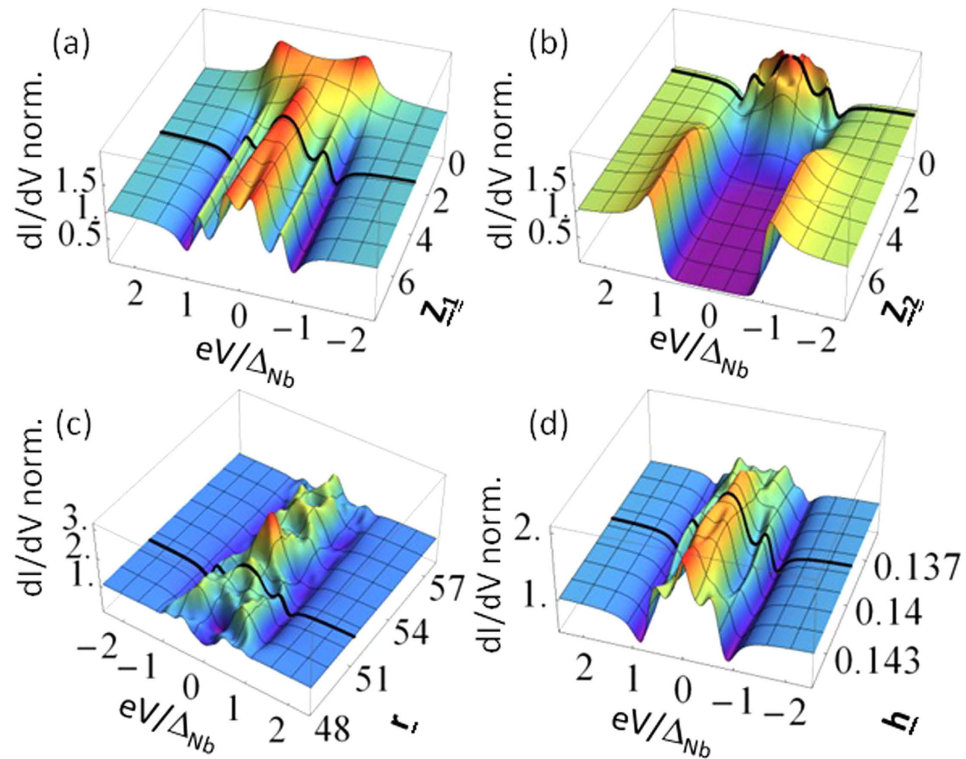


Figure 2. Evolution of the differential conductance spectra calculated using the theoretical model. The black spectrum evidenced in each plot is obtained for $Z_1 = 3.85$, $Z_2 = 0.35$, $r = 51.25$, $h = 0.1403$. Different plots are obtained by varying only one parameter (a) Z_1 , (b) Z_2 , (c) r , (d) h and keeping the other three parameters fixed.

verifying the correctness and the applicability of the model by comparison with the experimental results. Moreover, it is widely accepted that ballistic models can be properly used to explain the experimental results obtained in diffusive and/or granular systems, the only significant modification being a larger estimate of the BTK parameter (Z) associated to the interface transparency^{25,26}. Such considerations can be naturally extended to double barrier configurations in which resonant proximity effect is realized.

Conductance features versus model parameters. Hereafter, we show the conductance features originating from the theoretical model presented before. In discussing the results we use the dimensionless parameter r to characterize the ferromagnetic layer thickness d , taking the niobium Fermi momentum²⁷ $k_F^{Nb} \simeq 11.8 \text{ nm}^{-1}$ as the inverse of a reference length scale, i.e. $r = k_F^{Nb} \cdot d$. The remaining model parameters are the transparency of the N/F (F/S) interface Z_1 (Z_2) and the (intrinsic) polarization of the ferromagnetic layer $h = g\mu_B M/E_F$. The parameter h determines the number of spin up (down) electrons $n_\uparrow = \frac{n}{2}(1+h)$ ($n_\downarrow = \frac{n}{2}(1-h)$) expressed in terms of the total number of particles $n = n_\uparrow + n_\downarrow$, so that $P = (n_\uparrow - n_\downarrow)/(n_\uparrow + n_\downarrow) = h$.

Figure 2 shows the evolution of the conductance spectra as a function of the model parameters (Z_1 , Z_2 , r , h). The plots are obtained by keeping fixed three parameters and allowing only one parameter to vary in a range. Thus, we obtain Fig. 2a for $0 < Z_1 < 8$, Fig. 2b for $0 < Z_2 < 8$, Fig. 2c for $48 < r < 58$, and Fig. 2d for $0.135 < h < 0.145$. The solid (black) spectrum, in each panel, corresponds to a reference curve with the model parameters fixed as $Z_1 = 3.85$, $Z_2 = 0.35$, $r = 51.25$, $h = 0.1403$.

A completely transparent contact ($Z_1 = 0$) results in a simple spectrum with two maxima close to the gap energy (see Fig. 2a). Increasing Z_1 , there is a slow evolution of the spectra with the appearance of two conductance minima at $\pm\Delta_{Nb}$ and a Zero Bias Conductance Peak (ZBCP) accompanied by two maxima within energy gap. For large Z_1 values, the zero bias peak further splits. Differently, by varying Z_2 , the wide variety of conductance features appears only for transparent F/S barriers ($Z_2 < 1$), larger Z_2 values causing fully gapped spectra. Thus, the transparent regime is a necessary condition to observe the discussed features. We also notice that in the range $Z_2 < 1$ the conductance spectra show a moderate dependence on Z_2 (Fig. 2b) with respect to the spectra evolution originated by the remaining parameters (Fig. 2a,c,d). Moreover, the N-F/S configuration favors the formation of bound states in the F-layer²⁸ that appear in the differential conductance spectra as subgap resonances. The presence of such states is confirmed by an oscillating behaviour of the ZBC as a function of the r -parameter, as observed in

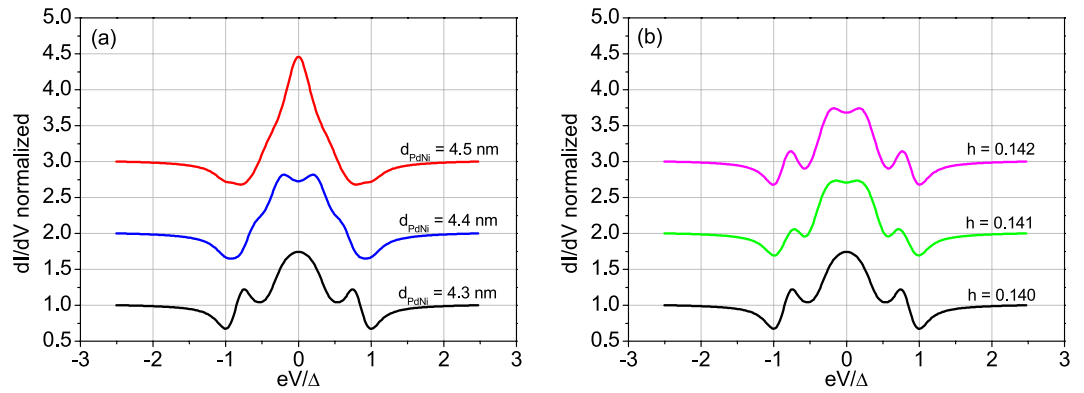


Figure 3. Comparison of conductance spectra calculated for small variations of the parameter (a) r and (b) h . The lower (black) spectrum in both panels is the reference conductance spectrum of Fig. 2. In (a) d_{PdNi} corresponds to r values according to $r = k_F^{\text{Nb}} \cdot d_{\text{PdNi}}$ with $k_F^{\text{Nb}} \simeq 11.8 \text{ nm}^{-1}$.

Fig. 2c. Indeed, since the emergence of these states is explained in terms of a width-dependent resonance condition, a ZBC modulation is expected by varying the confining dimension (i.e., F-layer thickness parametrized by r).

From Fig. 2c we notice a strong dependence of the conductance features on the parameter r , which can be used for the measurement of the F-layer thickness. The range $48 < r < 58$ corresponds to a thickness variation of the ferromagnetic layer of less than 1 nm. As an example, in Fig. 3a we show the different spectra obtained for $r = 51.25$ (i.e. $d \simeq 4.3 \text{ nm}$), $r = 52.25$ (i.e. $d \simeq 4.4 \text{ nm}$) and $r = 53.25$ (i.e. $d \simeq 4.5 \text{ nm}$). To complete the analysis of the conductance spectra dependence on the various parameters, we show in Fig. 2d the result obtained by varying h in the range $0.135 < h < 0.145$. This parameter gives direct information about the spin polarization P . The fast modification of the spectra for small variations of the parameter allows precise estimation of P . According to Fig. 3b, the differential conductance features are sensitive to h variations of the order of 10^{-3} .

Point contact spectroscopy. We apply the model to the results obtained in a point contact experiment where we realized a N-F/S device by pushing a gold tip on a PdNi(4 nm)/Nb(40 nm) bilayer. The experimental details concerning the setup and sample preparation and characterization are given in the Methods section.

In Fig. 4, we show a variety of normalized conductance spectra, obtained at $T = 4.2 \text{ K}$. In some cases, the spectra are characterized by a ZBCP higher than 2 (i.e., $G(V=0)/G_{\text{NN}} > 2$, where $G(V=0)$ is the conductance at zero bias, i.e. exceeding the maximum zero bias conductance value ($G(V=0)/G_{\text{NN}} = 2$) expected for a transparent barrier ($Z = 0$) in the standard BTK formulation. Moreover, double conductance dips as well as subgap maxima, with different intensity, are also observed.

To quantitatively analyze the conductance curves reported in Fig. 4a–d, experimental data are compared to theoretically calculated spectra. The fitting parameters are: the N/F barrier strength Z_1 , the F/S barrier strength Z_2 , the thickness parameter r and the spin polarization h ; superconducting energy gap and the effective temperature being fixed at the values $\Delta_{\text{Nb}}(0) \simeq 1.24 \text{ meV}$ (corresponding to the bulk value expected for a reduced $T_c \simeq 7.35 \text{ K}$, see Methods for details) and $T_{\text{eff}} = 0.7 \text{ K}$ (lower than the bath temperature of 4.2 K).

We notice that some reported conductance features appear too sharp compared to the expected thermal smearing, and require an effective temperature T_{eff} lower than the bath temperature. Such phenomenon has been already observed for Cu/Nb contacts⁷ and it has been ascribed to possible non-equilibrium transport processes in presence of proximity effect at the interface. Also considering the influence of cooling effect as reported²⁹ in N-F/S configuration, the cooling power generally acting on these systems seems to be not enough to cause a temperature reduction of few Kelvin, suggesting that further physical effects should contribute to determine such experimental observation. Alternatively, it has also been predicted that *extraordinary* temperature dependence of the resonant Andreev reflection peak is expected in N/quantum-dot/S systems³⁰, the tunneling mediated by discrete energy levels being responsible for an anomalous broadening of the conductance peak with respect the thermal one. Experimentally, such behavior has been reported for N/semiconductor/S systems³¹ and in N/High-Tc-Superconductors constrictions³², where the discrete levels could be due to the existence of surface (Andreev) bound states. However, a satisfactory explanation of such effective temperature is still lacking.

All conductance spectra are characterized by a large Z_1 value ($2.3 < Z_1 < 5.1$) indicating a low transparency of the contact between the gold tip and the PdNi layer; at the same time, significantly lower Z_2 values are always found ($0.26 < Z_2 < 0.50$) as expected for *in-situ* fabricated PdNi/Nb interface. The extracted Z_2 values confirm that in order to observe these conductance features a transparent F/S barrier

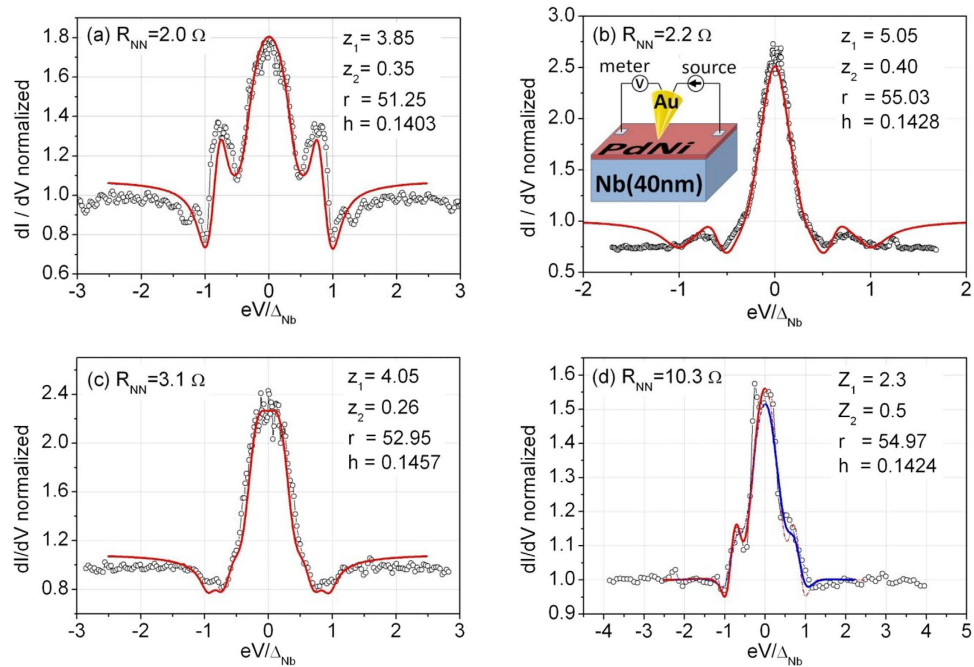


Figure 4. Differential conductance spectra, measured on different contacts at $T = 4.2$ K. Spectra are classified by R_{NN} , i.e. the high bias resistance. Inset in (b) shows a scheme of the setup. Data are normalized to $G_{NN} = 1$ (where $G_{NN} = 1/R_{NN}$) and compared to curves (solid lines) resulting from the theoretical model. Parameters used to reproduce the data are listed in each plot. All fits are performed by considering a temperature value $T_{eff} = 0.7$ K. (d) The asymmetry of the spectrum is reproduced by simply assuming a higher temperature for the positive energy side $T_{eff} = 1.1$ K.

is necessary. According to Fig. 4, we can notice that reported spectra are reproduced by $Z_2 \simeq 0.4 \pm 0.1$. The lowest value ($Z_2 = 0.26$, Fig. 4c) can be explained either in terms of the slow dependence of the conductance spectra on Z_2 or considering a local variation of the barrier properties (interface roughness, defects, etc.) due to the fabrication process. More interestingly, the remaining parameters involved in the fitting procedure take values in narrow intervals, $51.2 < r < 55.1$ and $0.140 < h < 0.146$, from which it is possible to give an estimation of the ferromagnet thickness $4.3 \text{ nm} < d < 4.6 \text{ nm}$ in the various sample positions and of the corresponding spin polarization $14.0\% < P < 14.6\%$. This finding is compatible with polarization values already reported in literature³³.

In order to verify that conductance features are strictly related to the superconductivity of niobium, we performed complete temperature dependence of the conductance spectra. We show in Fig. 5 that for $T = 7.7$ K the device is not anymore superconducting and all conductance features are washed out. Moreover, the conductance dip position (black arrows in Fig. 5a) and the amplitude of the zero bias peak both correctly follow the expected BCS behaviour for $\Delta(T)/\Delta(0) \approx \tanh\left[1.74\sqrt{\frac{T_c}{T} - 1}\right]$, see Fig. 5b,c.

It's worth mentioning that we used the minimal number of parameters to describe the physical system, where the existence of two interfaces (N/F and F/S parametrized by Z_1 and Z_2 , respectively) and the ferromagnetic properties of the F-layer (thickness and polarization parametrized respectively by r and h) are the quantities governing the device physics. Despite the number of parameters, the high sensitivity of the conductance features on the parameter evolution excludes the possibility of degenerate fittings as it has been widely verified during data analysis.

Discussion

In summary, using the Bogoliubov-de Gennes formalism, we studied the transport properties of N-F/S device in which thin ferromagnetic layer (of the order of ξ_F) is deposited on superconducting electrode, realizing a double-barrier structure. The spectroscopic features (i.e., differential conductance spectra) calculated within the theoretical model show a sensitive dependence on the ferromagnet properties (thickness and polarization). This peculiar behavior, originated by the resonant proximity effect, suggests the possibility to use Resonant Andreev Spectroscopy on F/S bilayer as a powerful characterization method to precisely probe local ferromagnetic properties. As a preliminary test of the theoretical expectations, we realized point contact Andreev reflection spectroscopy experiment by pushing a metallic tip on PdNi/Nb bilayer. Differential conductance spectra for several contacts have been measured at

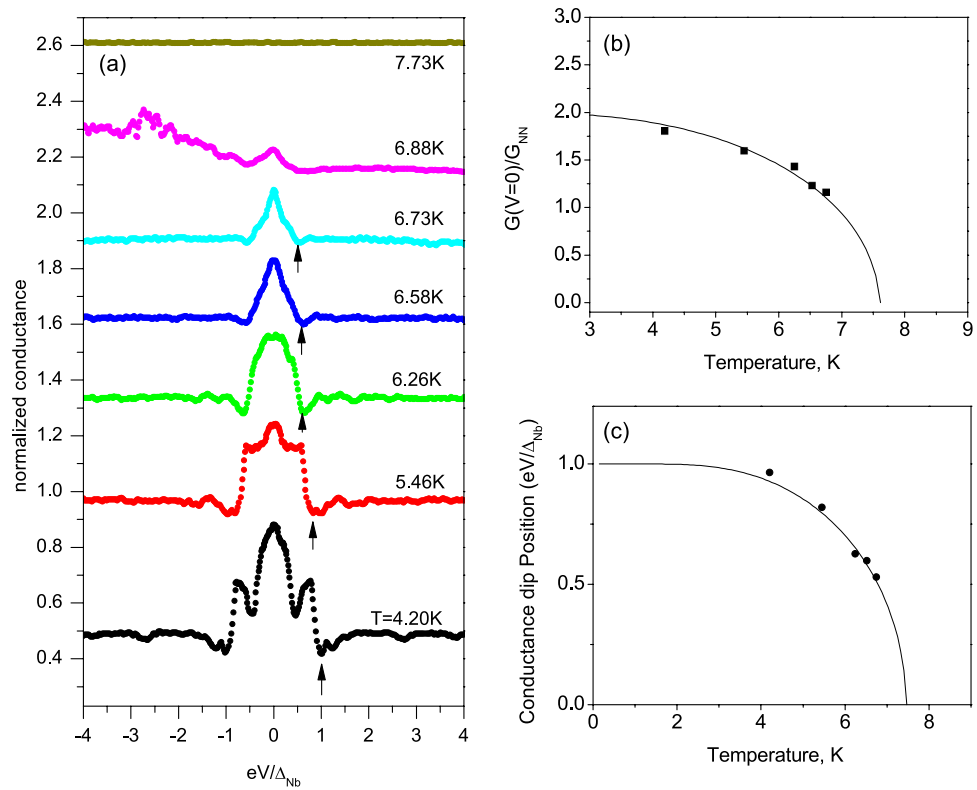


Figure 5. Temperature dependence of the conductance spectrum of Fig. 4a. (a) Curves have been shifted for clarity. Black arrows identify the position of the conductance dip at the gap edge. (b) Temperature evolution of the relative amplitude of the zero bias conductance $G(V=0)/G_{NN}$ is compared with the theoretical BCS behavior of $\Delta(T)$. (c) Temperature evolution of the conductance dip position. Solid line representing $\Delta(T)/\Delta(0)$ is reported for comparison.

low temperature, showing a variety of features (ZBCP, conductance dips at the gap edge, and subgap structures) not expected in single-barrier PCAR theories. Theoretical fittings allowed to consistently explain all measurements: ferromagnet quantities, namely the thickness and the polarization, have been estimated in accordance with the characterization measurements and the relevant literature.

Methods

The F/S bilayers were grown *in-situ* by a three-target ultra-high vacuum dc magnetron sputtering on Al_2O_3 substrates ($5\text{ mm} \times 5\text{ mm}$) in Argon pressure (few μbar) depositing first a 40 nm thick Nb layer and then a 4 nm thick $Pd_{0.84}Ni_{0.16}$ layer. Resistive transition measurements showed that the critical temperature of the bilayer was about 7.2 K compared to $T_c^{Nb} = 8.2\text{ K}$ of a reference (40 nm thick) Nb film. Magnetic and transport characterization of the bilayers has been widely addressed in previous works^{34–36} estimating $\xi_F = 3\text{--}4\text{ nm}$ ^{35,37}, i.e. the length scale over which the oscillation^{37–42} of the superconducting order parameter is expected in the F-side of the S/F bilayer. The thickness of the ferromagnetic layer covering the superconductor has been chosen to meet the condition $d \approx \xi_F$, in order to favor the coherent interplay between magnetic and superconducting correlations.

PCAR experiments have been performed by pushing a mechanically etched gold tip on the ferromagnetic side of the PdNi/Nb bilayer. The tip is installed on a screw driven chariot to gently approach the sample. The inset is introduced in a liquid helium cryostat to measure current-voltage (I-V) characteristics in the temperature range between 4.2 K and 10 K by conventional four-probe technique. Differential conductance spectra are obtained by numerical derivative. By varying the position and the pressure of the tip on the sample we obtained contact resistances in the range $2\ \Omega\text{--}10\ \Omega$. The transport regime through the contact can be easily estimated by using Wexler's formula⁴³ $R = 4\rho l/(3\pi a^2) + \rho/(2a)$ in which the first term gives the Sharvin resistance⁴⁴ describing the ballistic regime and the second one is the Maxwell⁴⁵ resistance describing the diffusive regime. The dominating term will depend on the contact dimension a , the resistivity ρ of the sample and the mean free path l of the charge carriers. For $\rho = 13\ \mu\Omega\text{cm}$ (as resulting by direct measurements) and considering that $\rho l = 3.72 \times 10^{-6}\ \mu\Omega\text{cm}^2$ for niobium^{46,47}, it comes out that the minimum contact dimension is $a \approx 8\text{ nm}$. The ratio $l/a < 1$ gives indication for diffusive contact.

However, the extension of BTK theory to diffusive contact has been proven^{25,26,48} to correctly identify the effect of P on the conductance spectra.

The observation of conductance dips has been often ascribed to the formation of thermal contacts. On the other hand, they have also been reported in presence of F/S and N/S point contacts experiments in which the thermal heating is excluded^{5,49–51}. We do exclude the thermal regime due to experimental evidences in the data. In fact, in the thermal regime, a reduced gap energy is expected⁵² with respect the bulk value, while no evidence of gap reduction is found. Moreover, as reported in ref. 52, the presence of heating effects implies a rising spectroscopic background already at $2\Delta_{Nb}$ while we report a flat background well visible up to four times the gap energy. A further experimental observation against the possible formation of a thermal contact is given in Fig. 3 where temperature dependence of conductance spectra is reported. According to D. Daghero *et al.*⁵³ the presence of temperature independent high energy tails of the conductance spectra as well as the Andreev signal disappearing at the same critical temperature measured for the bulk system by resistivity characterization demonstrate that the contact resistance has no contribution due to the Maxwell term.

References

- Johnson, P. D. Spin-polarized photoemission. *Rep. Prog. Phys.* **60**, 1217–1304 (1997).
- Meservey, R. & Tedrow, P. M. Spin-polarized electron tunneling. *Phys. Rep.* **283**, 173–243 (1994).
- de Jong, M. J. M. & Beenakker, C. W. J. Andreev Reflection in Ferromagnet-Superconductor Junctions. *Phys. Rev. Lett.* **74**, 1657–1660 (1995).
- Andreev, A. F. The Thermal Conductivity of the Intermediate State in Superconductors. *Sov. Phys. JETP* **19**, 1228–1231 (1964).
- Soulen, R. J. *et al.* Measuring the Spin Polarization of a Metal with a Superconducting Point Contact. *Science* **282**, 85–88 (1998).
- Upadhyay, S. K., Palanisami, A., Louie, R. N. & Buhrman, R. A. Probing Ferromagnets with Andreev Reflection. *Phys. Rev. Lett.* **81**, 3247–3250 (1998).
- Strijkers, G. J., Ji, Y., Yang, F. Y., Chien, C. L. & Byers, J. M. Andreev reflections at metal/superconductor point contacts: Measurement and analysis. *Phys. Rev. B* **63**, 104510 (2001).
- Kant, C. H., Kurnosikov, O., Filip, A. T., LeClair, P., Swagten, H. J. M. & De Jonge, W. J. M. Origin of spin-polarization decay in point-contact Andreev reflection. *Phys. Rev. B* **66**, 212403 (2002).
- Nadgorny, B. *et al.* Transport spin polarization of Ni_xFe_{1-x} : Electronic kinematics and band structure. *Phys. Rev. B* **61**, R3788–R3791 (2000).
- Nadgorny, B. *et al.* Origin of high transport spin polarization in $La_{0.7}Sr_{0.3}MnO_3$: Direct evidence for minority spin states *Phys. Rev. B* **63**, 184433 (2001).
- Ji, Y., Chien, C. L., Tomioka, Y. & Tokura, Y. Measurement of spin polarization of single crystals of $La_{0.7}Sr_{0.3}MnO_3$ and $La_{0.6}Sr_{0.4}MnO_3$. *Phys. Rev. B* **66**, 012410 (2002).
- Raychaudhuri, P., Mackenzie, A. P., Reiner, J. W. & Beasley, M. R. Transport spin polarization in $SrRuO_3$ measured through point-contact Andreev reflection. *Phys. Rev. B* **67**, 020411(R) (2003).
- Nadgorny B. *et al.* Measurements of spin polarization of epitaxial $SrRuO_3$ thin films. *Appl. Phys. Lett.* **82**, 427–429 (2003).
- DeSisto, W. J., Broussard, P. R., Ambrose, T. F., Nadgorny, B. E. & Osofsky M. S. Highly spin-polarized chromium dioxide thin films prepared by chemical vapor deposition from chromyl chloride. *Appl. Phys. Lett.* **76**, 3789–3791 (2000).
- Löfwander, T., Grein, R. & Eschrig, M. Is CrO_2 Fully Spin Polarized? Analysis of Andreev Spectra and Excess Current. *Phys. Rev. Lett.* **105**, 207001 (2010).
- Blonder, G., Tinkham, M. & Klapwijk, T. Transition from metallic to tunneling regimes in superconducting microrestrictions: excess current, charge-imbalance and supercurrent conversion. *Phys. Rev. B* **25**, 4515–4532 (1982).
- Peréz-Willard F. *et al.* Determining the current polarization in Al/Co nanostructured point contacts. *Phys. Rev. B* **69**, 140502(R) (2004).
- De Gennes, P. G. *Superconductivity of metals and alloys*. (Addison-Wesley Publishing Company, 1966).
- Volkov, A. F., Zaitsev, A. V. & Klapwijk, T. M. Proximity effect under nonequilibrium conditions in double-barrier superconducting junctions. *Physica C* **210**, 21–34 (1993).
- Yokoyama, T., Tanaka, Y. & Golubov, A. A. Resonant proximity effect in normal metal/diffusive ferromagnet/superconductor junctions. *Phys. Rev. B* **73**, 094501 (2006).
- Cottet, A., Huertas-Hernando, D., Belzig, W. & Nazarov, Yu. V. Spin-dependent boundary conditions for isotropic superconducting Green's functions. *Phys. Rev. B* **80**, 184511 (2009).
- Tanaka, Y. & Kashiwaya, S. Theory of Tunneling Spectroscopy of d-Wave Superconductors. *Phys. Rev. Lett.* **74**, 3451–3454 (1995).
- Wei, J. Y. T., Yeh, N.-C., Garrigus, D. F. & Strasik, M. Directional Tunneling and Andreev Reflection on $Yb_2Cu_3O_{7-\delta}$ Single Crystals: Predominance of d-Wave Pairing Symmetry Verified with the Generalized Blonder, Tinkham, and Klapwijk Theory. *Phys. Rev. Lett.* **81**, 2542–2545 (1998).
- Daghero, D. & Gonnelli, R. S. Probing multiband superconductivity by point-contact spectroscopy. *Supercond. Sci. Technol.* **23**, 043001 (2010).
- Woods, G. T. *et al.* Analysis of point-contact Andreev reflection spectra in spin polarization measurements. *Phys. Rev. B* **70**, 054416 (2004).
- Chen, T. Y., Huang, S. X. & Chien, C. L. Pronounced effects of additional resistance in Andreev reflection spectroscopy. *Phys. Rev. B* **81**, 214444 (2010).
- Ashcroft, N. W. & Mermin, N. D. *Solid State Physics*. (Brooks Cole, New York, 1976).
- Xu, J. H., Müller, J. H. & Ting, C. S. Conductance anomalies in a normal-metal-d-wave superconductor junction. *Phys. Rev. B* **53**, 3604–3612 (1996).
- Giazotto, F., Taddei, F., Fazio, R. & Beltram, F. Ultraefficient cooling in ferromagnet/superconductor microrefrigerators. *Appl. Phys. Lett.* **80**, 3784–3786 (2002).
- Zhu, Y., Sun, Q. & Lin, T. Extraordinary temperature dependence of the resonant Andreev reflection. *Phys. Rev. B* **64**, 134521 (2001).
- Magnée, P. H. C., van der Post, N., Kooistra, P. H. M., Van Wees, B. J. & Klapwijk, T. M. Enhanced conductance near zero voltage bias in mesoscopic superconductor-semiconductor junctions. *Phys. Rev. B* **50**, 4594–4599 (1994).
- Dagan, Y., Kohen, A., Deutscher, G. & Revcolevschi, A. Absence of Andreev reflections and Andreev bound states above the critical temperature. *Phys. Rev. B* **61**, 7012–7016 (2000).
- Arham, H. Z., Khaire, T. S., Loloee, R., Pratt, W. P. & Birge, N. O. Measurement of spin memory lengths in PdNi and PdFe ferromagnetic alloys. *Phys. Rev. B* **80**, 174515 (2009).

34. Cirillo C. *et al.* Superconducting proximity effect and interface transparency in Nb/PdNi bilayers. *Phys. Rev. B* **72**, 144511 (2005).
35. Cirillo, C., Ilyina, E. A. & Attanasio, C. Static and dynamic properties of the vortex lattice in superconductor/weak ferromagnet bilayers. *Supercond. Sci. Technol.* **24**, 024017 (2011).
36. Romano, P., Polcari, A., Cirillo, C. & Attanasio, C. Non-monotonic behaviour of the superconducting order parameter in Nb/PdNi bilayers observed through point contact spectroscopy. *Supercond. Sci. Technol.* **25**, 095017 (2012).
37. Fominov, Ya. V., Chtchelkatchev, N. M. & Golubov, A. A. Nonmonotonic critical temperature in superconductor/ferromagnet bilayers. *Phys. Rev. B* **66**, 014507 (2002).
38. Radović, Z., Ledvij, M., Dobrosavljević-Grujić, L., Buzdin, A. I. & Clem, J. R. Transition temperatures of superconductor-ferromagnet superlattices. *Phys. Rev. B* **44**, 759–764 (1991).
39. Jiang, J. S., Davidović, D., Reich, D. H. & Chien, C. L. Oscillatory Superconducting Transition Temperature in Nb/Gd Multilayers. *Phys. Rev. Lett.* **74**, 314–317 (1995).
40. Zdravkov V. *et al.* Reentrant Superconductivity in Nb/Cu_{1-x}Ni_x Bilayers. *Phys. Rev. Lett.* **97**, 057004 (2006).
41. Buzdin, A. Density of states oscillations in a ferromagnetic metal in contact with a superconductor. *Phys. Rev. B* **62**, 11377–11379 (2000).
42. Kontos, T., Aprili, M., Lesueur, J. & Grison, X. Inhomogeneous Superconductivity Induced in a Ferromagnet by Proximity Effect. *Phys. Rev. Lett.* **86**, 304–307 (2001).
43. Wexler, A. The size effect and the non-local Boltzmann transport equation in orifice and disk geometry. *Proc. Phys. Soc.* **89**, 927–941 (1966).
44. Sharvin, Y. V. On the possible method for studying Fermi surfaces. *Zh. Eksp. Teor. Fiz.* **48**, 984–985 (1965).
45. Maxwell, J. C. *Treatise on Electricity and Magnetism.* (Clarendon, Oxford, 1904).
46. Goodman, B. B. & Kuhn, G. J. Influence des défauts étendus sur les propriétés supraconductrices du niobium. *Phys. Paris* **29**, 240–252 (1968).
47. Garwin, E. L. & Rabinowitz, M. Resistivity Ratio of Niobium Superconducting Cavities. *Appl. Phys. Lett.* **20**, 154–156 (1972).
48. Mazin, I. I., Golubov, A. A. & Nadgorny, B. Probing spin polarization with Andreev reflection: A theoretical basis. *J. Appl. Phys.* **89**, 7576–7578 (2001).
49. DeGrave J. P. *et al.* Spin Polarization Measurement of Homogeneously Doped Fe_{1-x}Co_xSi Nanowires by Andreev Reflection Spectroscopy. *Nano Lett.* **11**, 4431–4437 (2011).
50. SanGiorgio, P., Reymond, S., Beasley, M. R., Kwon, J. H. & Char, K. Anomalous Double Peak Structure in Superconductor/Ferromagnet Tunneling Density of States. *Phys. Rev. Lett.* **100**, 237002 (2008).
51. Boden, K. M., Pratt, W. P. & Birge N. O. Proximity-induced density-of-states oscillations in a superconductor/strong-ferromagnet system. *Phys. Rev. B* **84**, 020510(R) (2011).
52. Blonder, G. E. & Tinkham, M. Metallic to tunneling transition in Cu-Nb point contacts. *Phys. Rev. B* **27**, 112–118 (1983).
53. Daghero, D. *et al.* Strong-coupling *d*-wave superconductivity in PuCoGa₅ probed by point-contact spectroscopy. *Nature Phys.* **3**, 786 (2012).

Author Contributions

F.R. developed theoretical model, performed numerical fittings, contributed to data analysis and wrote the paper; F.G. designed the experiment, performed PCAR measurements and numerical fittings, did data analysis and wrote the paper; R.C. contributed to develop the theoretical model; A.D.B. and A.P. helped with the data analysis; C.C. and C.A. provided the bilayers and their electrical characterization; P.R. contributed to the experiment design, measurements and data analysis. The manuscript was revised by all authors. All authors have given approval to the final version of the manuscript.

Additional Information

Competing financial interests: The authors declare no competing financial interests.

How to cite this article: Romeo, F. *et al.* Resonant Andreev Spectroscopy in normal-Metal/thin-Ferromagnet/Superconductor Device: Theory and Application. *Sci. Rep.* **5**, 17544; doi: 10.1038/srep17544 (2015).



This work is licensed under a Creative Commons Attribution 4.0 International License. The images or other third party material in this article are included in the article's Creative Commons license, unless indicated otherwise in the credit line; if the material is not included under the Creative Commons license, users will need to obtain permission from the license holder to reproduce the material. To view a copy of this license, visit <http://creativecommons.org/licenses/by/4.0/>